Biomaterials 35 (2014) 3744–3755

Contents lists available at ScienceDirect

Biomaterials

journal homepage: www.elsevier.com/locate/biomaterials

Corneal stromal bioequivalents secreted on patterned silk substrates

Jian Wu [a], Jelena Rnjak-Kovacina [b], Yiqin Du [c], Martha L. Funderburgh [c], David L. Kaplan [b], James L. Funderburgh [a,c,*]

[a] McGowan Institute for Regenerative Medicine and Department of Surgery, University of Pittsburgh School of Medicine, Pittsburgh, PA, USA
[b] Department of Biomedical Engineering, Tufts University, Medford, MA, USA
[c] Department of Ophthalmology, University of Pittsburgh School of Medicine, Pittsburgh, PA, USA

ARTICLE INFO

Article history:
Received 28 October 2013
Accepted 23 December 2013
Available online 3 February 2014

Keywords:
Stem cells
Keratocytes
Corneal fibroblasts
RGD
Silk
Cornea

ABSTRACT

Emulating corneal stromal tissue is believed to be the most challenging step in bioengineering an artificial human cornea because of the difficulty in reproducing its highly ordered microstructure, the key to the robust biomechanical properties and optical transparency of this tissue. We conducted a comparative study to assess the feasibility of human corneal stromal stem cells (hCSSCs) and human corneal fibroblasts (hCFs) in the generation of human corneal stromal tissue on groove-patterned silk substrates. In serum-free keratocyte differentiation medium, hCSSCs successfully differentiated into keratocytes secreting multilayered lamellae with orthogonally-oriented collagen fibrils, in a pattern mimicking human corneal stromal tissue. The constructs were 90–100 μm thick, containing abundant cornea-specific extracellular matrix (ECM) components, including keratan sulfate, lumican, and keratocan. In contrast, hCFs tended to differentiate into myofibroblasts that deposited less organized collagen in a pattern resembling that of corneal scar tissue. RGD surface coupling coupling was an essential factor in enhancing cell attachment, orientation, proliferation, differentiation and ECM deposition on the silk substratum. These results demonstrated that an approach of combining hCSSCs with an RGD surface-coupled patterned silk film offers a powerful tool to develop highly ordered collagen fibril-based constructs for corneal regeneration and corneal stromal tissue repair.

1. Introduction

The cornea provides essential features to the visual system, including optical transparency, biological and mechanical protection, and light refraction. Once the cornea loses transparency due to scarring or disease, corneal transplantation (penetrating keratoplasty, PK) is the prevailing option to correct visual impairment. In USA, there are 30,000–40,000 PK operations performed every year [1]. Although short-term success of this procedure is high, long-term (i.e. >10 year) graft survival is similar to that of other organ transplants, 64% [2]. Once a transplanted cornea is rejected, a subsequent graft is at high risk for rejection. The increasing use of Laser-Assisted In Situ Keratomileusis (LASIK) surgery for refractive correction has reduced the availability of donor corneas and in many parts of the world, donor tissues are in short supply or not available. This shortage of healthy corneal donor tissue has stimulated efforts to develop biological human corneal equivalents employing a tissue engineering strategy [3–5].

Synthetic corneal prostheses are in limited use and recombinant collagen is in clinical trials for partial thickness keratoplasty [6], but there are currently no clinically viable cellularized human corneal equivalents produced by tissue engineering methods. A major challenge in bioengineering a cornea is in producing a biological equivalent of the corneal stroma. This tough, optically transparent tissue is made up of 300–500 lamellae composed of tightly-packed, highly aligned collagen fibrils with uniform fibril size and interfibril spacing. This complex, hierarchical microstructure is principally responsible for optical transparency and biomechanical properties of human cornea [7–9] and is challenging to recapitulate *in vitro*.

Silk fibroin, mainly produced from *Bombyx mori* silkworm cocoons, has been extensively introduced as biomaterial scaffolds for tissue engineering and regenerative medicine due to its biocompatibility [10,11], controllable degradability [12,13], tunable mechanical properties [14,15] and low immunogenicity [11,16]. Because of its optical transparency, silk fibroin film has previously been used in ocular tissue reconstruction [17,18]. Silk fibroin membranes have been shown to support the growth of corneal epithelial cells [19–21], corneal endothelial cells [22], and retinal pigment epithelial cells [23]. Preclinical *in vivo* studies in a rabbit

* Corresponding author. Department of Ophthalmology, University of Pittsburgh School of Medicine, Pittsburgh, PA, USA. Tel.: +1 412 647 3853; fax: +1 412 647 5880.
E-mail address: jlfunder@pitt.edu (J.L. Funderburgh).

0142-9612/$ – see front matter © 2014 Elsevier Ltd. All rights reserved.
http://dx.doi.org/10.1016/j.biomaterials.2013.12.078

model demonstrated that the transparent porous silk membranes are a promising carrier for cultivated epithelial sheets in the regeneration of corneal epithelium [24]. Coupled with Arginine-Glycine-Aspartic acid (RGD) peptide cell-receptor motif and groove-patterned surface, silk films efficiently support corneal fibroblast attachment, orientation, proliferation, enhanced corneal stroma gene expression and deposition of aligned fibrillar collagen [25–27]. RGD-coupled silk films also improve attachment and differentiation of mesenchymal stem cells [28].

Keratocytes are native resident cells of the corneal stroma, principally responsible for the maintenance of the transparent stromal tissue by secreting a spectrum of unique matrix molecules [29–32]. Expansion of keratocytes *in vitro* inevitably leads to their differentiation into corneal fibroblasts [29,30,32,33]. Corneal fibroblasts exhibit a wound-healing phenotype and secrete disorganized extracellular matrix (ECM) typically found in corneal scars [29,30,32]. The discovery and isolation of human corneal stromal stem cells (hCSSCs) [34–37] make it possible to mimic the developmental process and generate stromal tissue *in vitro*. Du et al. demonstrated that hCSSCs maintain the potential to become keratocytes through a large number of population doublings [36]. Different from corneal fibroblasts, hCSSCs can produce abundant ECM containing cornea stroma-specific components, keratan sulfate and keratocan [35]. In this study, we compared the applicability of human corneal stromal stem cells (hCSSCs) versus human corneal fibroblasts (hCFs) in the generation of human corneal stromal tissue on patterned silk fibroin membranes.

2. Materials and methods

2.1. Preparation of regenerated silk fibroin solution

Silk fibroin solution was prepared according to previously reported methods [38]. Briefly, 5 g of *B. mori* silkworm cocoons (Tajima Shoji Co., LTD, Japan) were degummed in 2 L of boiling 0.02 M sodium carbonate for 30 min to remove the sericin protein from the fiber. The degummed fibers were dissolved in a 9.3 M lithium bromide solution (20% wt/v) at 60 °C for 4 h. The dissolved silk solution was dialyzed against 4 L of ultrapure water in dialysis cassettes with a 3500 molecular weight (MW) cutoff (Pierce Biotechnology, Rockford, IL). Water was changed three times per day for three days. The dialyzed silk solution was centrifuged twice at 8800 rpm for 20 min and the supernatant collected at 4 °C.The concentration of the final silk solution (6–8% wt/v) was determined by gravimetric analysis.

2.2. Preparation of PDMS substrates

Patterned polydimethylsiloxane (PDMS, Sylgard 184 Silicone Elastomer Kit, Dow Corning, Midland, MI) substrates were prepared by casting PDMS on a reflective diffraction grating surface with linear 3.5 μm wide and 500 nm deep grooves (Edmund Optics, Inc, Barrington, NJ). The substrates were cut into 40 × 40 mm squares, washed in 70% v/v ethanol and thoroughly rinsed in distilled water before casting silk solution on the substrates to generate the patterned films.

2.3. Preparation of silk films

A 1.2 mL aliquot of 1% w/v silk solution was cast upon grooved PDMS molds resulting in 3 μm thick films after drying. The films were covered with a venting lid and allowed to dry overnight at room temperature. The as-cast films were water annealed in a vacuum oven with a 200 mL water tray at the bottom at 25 °C, 20 mmHg vacuum for 2 h. Dry silk films were wrapped in aluminum foil and autoclaved at 121 °C for 20 min to sterilize. The films were hydrated in distilled water, punched into 12 mm (diameter) constructs and placed in 24-well plates for cell seeding.

2.4. RGD surface modification

RGD coupling to silk film surface was carried out as previously described [27] under sterile conditions. The silk films were presoaked in BupH™ MES buffered saline, pH 6.0 (Thermo Scientific, Waltham, MA). The –COOH groups in silk fibroin were activated with 1-ethyl-3-(dimethylaminopropyl) carbodiimide hydrochloride (EDC–HCl)/N-hydroxysuccinimide (NHS) solution (0.5 mg/mL of EDC and 0.7 mg/mL of NHS in MES buffer, pH 6.0) for 30 min at room temperature, generating amine-reactive NHS-esters on the silk film surface. The activated silk films were washed with MES buffer three times and subsequently incubated in 1 mg/mL Glycine-Arginine-Glycine-Aspartic acid-Serine (GRGDS) peptide (Bachem, Torrance, CA) in MES buffer pH 6.0 for 2 h. After the GRGDS coupling reaction, the surface modified silk films were washed twice in MES buffer and five times in distilled water.

2.5. Culture of human corneal stromal stem cells and human corneal fibroblasts

Human corneal stromal stem cells (hCSSCs) were isolated from collagenase-digested limbal stromal tissue of human corneas unsuitable for transplant obtained from the Center for Organ Recovery & Education (Pittsburgh, PA), as previously described [36]. Cells at passage six were used for the experiments [39]. To prepare human corneal fibroblasts (hCFs) as a comparison, the isolated human corneal stromal keratocytes were expanded in DMEM/F-12 (Sigma–Aldrich) supplemented with 10% fetal bovine serum (FBS, Life Technologies). Passage 6 fibroblasts were used for the experiment [37].

Discs of sterile patterned silk film were cut and anchored in wells of 24-well culture plates using Silicone Rubber O-rings. hCSSCs and hCFs were seeded on the substratum at 5.0×10^4 cells/cm^2. hCSSCs were incubated with 1.0 mL of stem cell growth medium containing DMEM/MCDB-201 with 2% fetal bovine serum, 10 ng/mL epidermal growth factor, 10 ng/mL platelet-derived growth factor (PDGF-BB), 5 μg/mL insulin, 5 μg/mL transferrin, 5 ng/mL selenous acid (ITS), lipid-rich bovine serum albumin (Albumax, Life Technologies, Grand Island, NY) 0.1 mM ascorbic acid-2-phosphate, 10^{-8} M dexamethasone, 100 IU/mL penicillin, 100 μg/mL streptomycin, 50 μg/mL gentamicin, 100 ng/ml cholera toxin until confluent (usually 3 days) [39,40]. hCFs were incubated in DMEM/F12 containing 10% FBS until confluence.

At confluence, cells were incubated in keratocyte differentiation medium (KDM) consisting of Advanced DMEM (Life Technologies) supplemented with 1.0 mM L-ascorbic acid-2-phosphate (Sigma–Aldrich, St Louis, MO), 2 mM L-alanyl-L-glutamine (GlutaMax™-1, Life Technologies), 50 μg/mL gentamicin (Life Technologies), 100 μg/mL penicillin, 100 μg/mL streptomycin (Mediatech, Manassas, VA), 10 ng/mL basic fibroblast growth factor (FGF-2, Sigma–Aldrich) and 0.1 ng/mL transforming growth factor-beta3 (TGF-β3, Sigma–Aldrich) [40]. The medium was changed twice per week for up to 9 weeks.

2.6. Two-photon fluorescent microscopy

Multiphoton imaging was performed employing an Olympus FV1000 multiphoton microscope (Center Valley, PA). It is an upright fixed stage microscope equipped with a large area motorized stage. Samples were set in a custom built imaging chamber, and three-dimensional image sets collected with a 25 × 1.0 NA objective specifically designed for multiphoton microscopy. The microscope laser with wavelength of 830 nm was utilized to collect the second harmonic generation (SHG) signal of collagen fibrils. The images were collected as three-dimensional data sets (section spacing 2 μm), with the number of sections in each stack varying from specimen to specimen. Image stacks once collected were processed into three-dimensional stacks using Imaris (Bitplane, South Windsor, CT).

2.7. Electron microscopy

Specimens for electron microscopy imaging were prepared as described previously [37,39]. Briefly, all of the specimens were fixed in cold 2.5% glutaraldehyde (EM grade, Taab Chemical, Aldermaston, England) in 0.1 M PBS, pH 7.3. The specimens were rinsed in PBS, post-fixed in 1% osmium tetroxide (Electron Microscopy Sciences, Hatfield, PA) with 0.1% potassium ferricyanide (Fisher Scientific, Pittsburg, PA), and dehydrated through a graded series of ethanol washes.

For the imaging of transmission electron microscopy (TEM), the dehydrated samples were embedded and cured in Epon (Energy Beam Sciences, East Granby, CT). Sections were cut perpendicular to the alignment of the underlying grooved substrates. Semi-thin sections (300 nm) were stained with 0.5% Toluidine Blue (Fisher) and examined under optical microscope equipped with CCD camera. Ultra-thin sections (65 nm) were stained with 2% uranyl acetate (Electron Microscopy Sciences) in a 1:1 mixture of water and methanol, and then with aqueous 1% phosphotungstic acid (Sigma–Aldrich), pH 3.2. The sections were examined and photographed with a Jeol 1011 transmission electron microscope (JEOL Ltd., Tokyo, Japan) working at 80 kV. For scanning electron microscopy (SEM), the dehydrated samples were chemically dried with hexamethyldisilazane for 15 min. The samples were imaged at 5 kV by a Jeol JSM-6330F Scanning Electron Microscope.

2.8. Gene expression

Gene expression was examined by quantitative RT-PCR (qPCR) as described previously [39]. In brief, DNAse-treated total RNA (400 ng) isolated from constructs (RNeasy, Qiagen, Valencia, CA) was transcribed to cDNA by SuperScript II reverse transcriptase (Life Technologies) using priming with random hexamers. Quantitative RT-PCR of cDNA equivalent to 20 ng RNA was performed with direct dye binding (SYBR Green; Applied Biosystems, Carlsbad, CA) according to the manufacturer's instruction. A dissociation curve for each SYBR-based reaction was generated to confirm that there was no nonspecific amplification. Amplification of 18S rRNA was conducted for each cDNA (in triplicate) for normalization of RNA content. Relative mRNA abundance was calculated as the cycle threshold (Ct) for amplification of a gene-specific cDNA minus the average Ct for 18S expressed as a power of 2 ($2^{-\triangle Ct}$). Three individual gene-specific values thus calculated were averaged to obtain a mean ± SD. Primer sequences were as previously published [36,41].

Six genes were selected which have previously been used to identify keratocyte phenotype. Keratocan (KERA) [33] and prostaglandin D2 synthase (PTGDS) [42] are keratan sulfate core proteins, unique molecular markers of the corneal stroma.

Corneal N-acetylglucosamine-6-O-sulfotransferase (CHST6) [43], is an enzyme involved in keratan sulfate synthesis. Corneal crystallin, aldehyde dehydrogenase 3A1 (ALDH) is a cell-associated protein highly expressed in cornea [44]. Smooth muscle alpha actin (α-SMA) and extra-domain A fibronectin (EDA-FN) are proteins not present in normal transparent stroma, rather they represent markers of fibrotic corneal scar tissue secreted in healing wounds by corneal myofibroblasts [33,41].

2.9. Whole-mount immunostaining

After 9 week of culture, the ECM deposited by hCSSCs and hCFs on patterned silk substrates was fixed in 2.5% paraformaldehyde (PFA) in PBS at room temperature for 20 min, rinsed 10 min in PBS three times, and stored at 4 °C in PBS for further processing. Except those for keratocan and lumican staining, the fixed samples were incubated in 10% heat-inactivated goat serum at room temperature for 1 h to block nonspecific binding, rinsed in PBS, and incubated with mouse monoclonal primary antibodies diluted with 1% bovine serum albumin (BSA, Fluka, St Louis, MO) in PBS overnight at 4 °C in a sealed moist box. For immunostaining of keratocan and lumican, the samples were first digested with keratanase (0.5 U/mL) (Sigma–Aldrich) in 1% BSA in PBS for 2 h at 37 °C, rinsed in PBS three times (10 min each), and then incubated with primary anti-human keratocan antibody and anti-human lumican antibody, respectively overnight at 4 °C, following three 10 min washes in PBS.

Primary antibodies used for immunostaining included anti-keratocan polyclonal peptide antibody (keratocan, Sigma–Aldrich), monoclonal antibody Lum-1 to lumican (provided by Bruce Caterson, Cardiff University, Wales, UK), monoclonal antibody J19 to keratan sulfate (gift from Nirmala SundarRaj, University of Pittsburgh, Pittsburgh, PA), anti-collagen I (Sigma–Aldrich), anti-collagen V (Chemicon) and anti-collagen VI (Chemicon) monoclonal antibodies.

For myofibroblast staining, fixed cells were first permeabilized with 0.1% Triton X-100 in PBS for 20 min and thoroughly washed by PBS. The permeabilized cells were labeled with Alexa-Fluor 488 phalloidin (2 μg/ml, Life Technologies), and incubated with mouse anti-human alpha-smooth muscle actin (α-SMA, 1:100, Sigma–Aldrich) overnight at 4 °C, then washed three time for 10 min with PBS.

Secondary antibody Alexa-Fluor 488-donkey anti-mouse or Alexa-Fluor 488 donkey anti-rabbit (1:2500) (Life Technologies) together with 4′,6-diamidino-2-phenylindole (DAPI) (0.5 ng/mL, Roche, Indianapolis, IN) was added to the samples, and incubated for 2 h at room temperature. The stained samples were placed in aqueous mounting medium (Thermo Fisher Scientific) and examined using an Olympus FluoView FV1000 confocal microscope.

2.10. Statistical analysis

Statistical comparisons were conducted by one way ANOVA followed by post-hoc Newman–Keuls multiple comparison testing to evaluate the influence of the cell types in which $p < 0.05$ was considered significant. All of the results pertaining to gene expression, construct thickness, collagen-fibril size and inter-fibrillar spacing are expressed as mean ± standard deviation.

3. Results

3.1. Cell morphology on patterned silk films

To provide a cell-guiding substrate for corneal tissue engineering, silk film surfaces were patterned with linear grooves employing soft lithography [25,45]. Scanning electron micrograph (SEM) of the patterned silk film is presented in Fig. 1a. The linear groove pattern was previously characterized and displays a saw tooth shape with grooves of 515 ± 16.0 nm depth and 3597 ± 89 nm width and overall roughness of 162.6 ± 2.0 nm [46]. The response of hCSSCs and hCFs to the patterned silk films was evaluated by Calcein AM staining and confocal laser-scanning microscopy. On membranes lacking RGD, corneal fibroblasts (hCF) did not adhere and grow, thus no further analyses of this combination of cells and substratum could be carried out (data not shown). Although hCSSC attached to the membranes without RGD surface modification, the cells did not align (Fig. 1b) and showed limited proliferation. After 3 days in SCGM culture hCSSCs still did not form a confluent cell layer in the absence of RGD modification (Fig. 1e). In contrast, the patterned silk film with RGD surface coupling guided hCSSCs (Fig. 1c) and hCFs (Fig. 1d) to elongate and align along the linear groove long axis (shown by arrow). After 3 days of culture, both cell types were confluent on the RGD-modified substrates. Morphologically, hCFs remained more elongated and spindle-like than hCSSCs. Furthermore, hCFs organized in orthogonally stratified manner (Fig. 1g) in some areas, while hCSSCs were fully confluent and aligned in a single orientation (Fig. 1f).

3.2. Gene expressions of hCSSCs and hCFs on silk films

After 3 days of proliferation, hCSSCs and hCFs were switched into serum-free keratocyte differentiation medium (KDM) containing 10 ng/mL FGF-2 and 0.1 ng/mL TGF-β3 [40]. Gene expression of hCSSCs and hCFs differentiated in KDM was examined by qPCR. Fig. 2 shows the gene expression patterns (normalized to 18S rRNA) of differentiated hCSSCs and hCFs as a function of culture

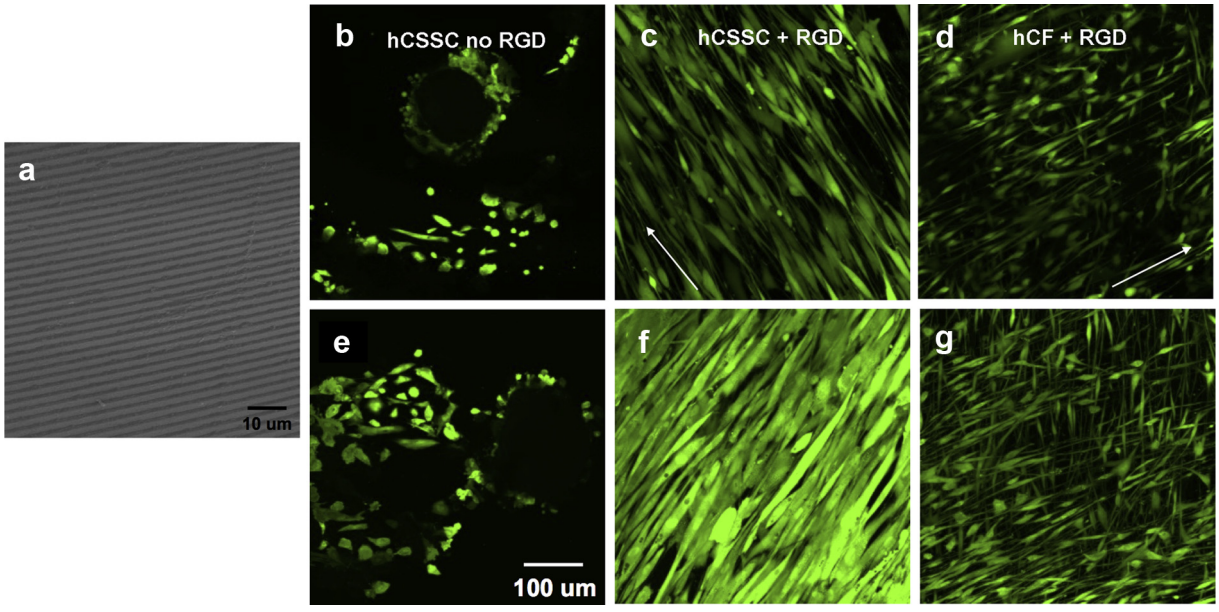

Fig. 1. Patterned, RGD-modified silk films induce cell alignment. A scanning electron micrograph shows the patterned silk film substratum (a). Confocal laser-scanning micrographs of hCSSCs grown on patterned silk films without (b, e) and with (c, f) RGD-surface modification. hCFs (d, g) grown on patterned silk films with RGD-surface modification. hCF cells plated on surfaces without RGD modification did not adhere (not shown). Day 1 of culture (b–d) and day 3 (e–g). Cells were labeled using fluorescent viability marker dye Calcein AM. Arrows indicate direction of grooves in the silk substratum.

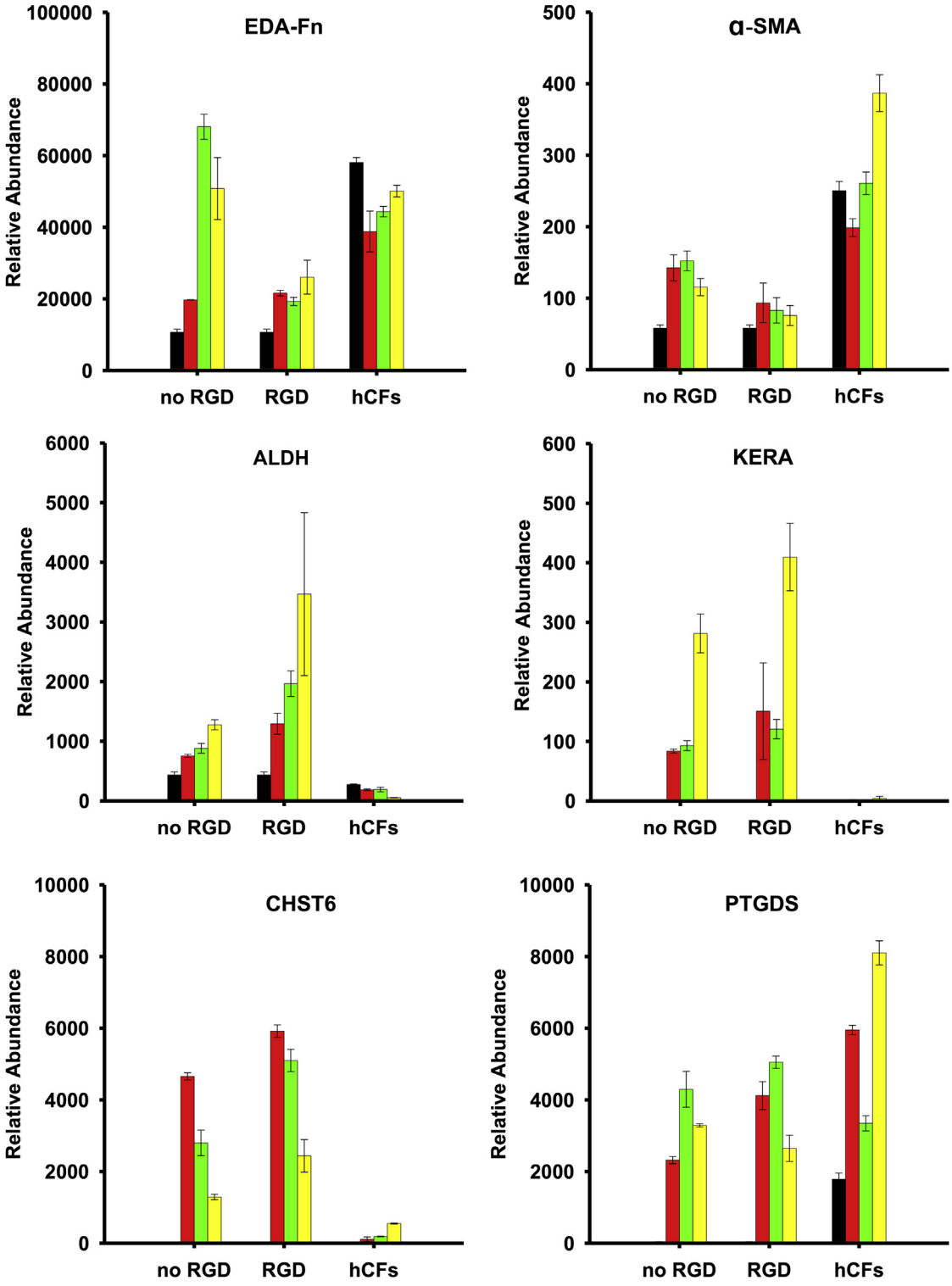

Fig. 2. Expression of mRNA in hCSSCs and hCFs during culture on patterned silk films. Expression levels of keratocyte genes were determined by qPCR as described in Methods. Bars show the relative abundance of gene-specific mRNA in comparison to 18S RNA. Black bars (▬), 0 weeks (i.e., control cells at time of plating); red bars (▬), 3 weeks culture; green bars (▬), 6 weeks; yellow bars (▬), 9 weeks culture. "No RGD" and "RGD" refer to hCSSCs seeded on patterned silk films without and with RGD-surface modification. hCFs refers to hCFs grown on RGD-modified patterned silk film. Error bars show SD of three independent samples. Expression of each gene significantly increased in hCSSC the cultured cells (colored bars) compared to the starting cells (black bars) ($p < 0.05$). Expression of KERA, CHST6, and ALDH in hCSSC + RGD was significantly greater than expression in hCF at all time points, whereas expression of alpha-SMA and EDA-FN was significantly less ($p < 0.05$). (For interpretation of the references to color in this figure legend, the reader is referred to the web version of this article.)

time. Initially, hCSSCs displayed no detectable expression of the characteristic gene markers of keratocytes including KERA (keratocan), CHST6 (corneal N-acetylglucosamine-6-O-sulfotransferase) and PTGDS (prostaglandin D2 synthase) when cultured in SCGM. After culture in KDM, expression of these keratocyte genes plus ALDH3A1 (Aldehyde dehydrogenase 3A1) was substantially upregulated and their expression increased over the 9-week culture period. Furthermore, RGD-surface coupling induced hCSSCs to express much higher levels of keratocyte-specific markers, and notably lower expression levels of EDA-FN and α-SMA, the two typical markers of myofibroblasts, compared to no hCSSC cultured on silk films without RGD modification.

hCFs had no detectable expression of KERA and CHST6 before culture in KDM. Different from hCSSCs, hCFs did not show a significant change in the gene expression of keratocyte-specific genes during the 9-week culture in KDM. Except for PTGDS, expression of other keratocyte markers, including KERA, ALDH3A1 and CHST6, was low compared with hCSSCs. In contrast, the expression of myofibroblast markers EDA-FN and α-SMA was substantially upregulated after differentiation. The tendency of cells toward myofibroblast differentiation was further investigated by immunohistochemistry staining.

3.3. Protein expression

After 9 weeks of culture in serum-free KDM, the presence and expression of α-SMA, a fibrotic marker, was investigated by con focal microscopy. On the patterned silk substrate *without* RGD-surface coupling, the differentiated hCSSCs surrounding the cellular sphere developed the prominent f-actin fibril bundles randomly organized within the cells as seen by phalloidin staining (Fig. 3a), and simultaneously showed strong expression of α-SMA (Fig. 3d). The hCSSCs differentiated on the substrate *with* RGD-surface coupling showed most f-actin stress fibers crossing the cells, and cortical actin was homogeneously distributed near the cell membrane (Fig. 3b). Simultaneously, α-SMA was not detected to any significant extent (Fig. 3e). Different from hCSSCs, hCFs on RGD-modified surfaces showed robust organization of f-actin stress fibrils throughout the cells aligned with the linearly patterned grooves of the substratum (Fig. 3c). The intracellular α-SMA expression in hCFs was much stronger than that in hCSSCs under the same conditions (Fig. 3f).

3.4. Extracellular matrix (ECM)

The expression of corneal stroma-specific collagens and proteoglycans in the extracellular matrix (ECM) was investigated by whole mount immunohistochemical examination. Collagen type-I (Col-1), collagen type-V (Col-V) and collagen type-VI (Col-VI) are representative collagens abundant in human corneal stromal tissue [47–51]. Without RGD surface coupling, differentiating hCSSC cells aggregated into spheroid bodies (Fig. 4a–c) containing cells and staining for each of these collagens. The ECM deposited by stellate cells surrounding the sphere had less collagen accumulation. On membranes with RGD surface coupling, the collagen fibrils were highly aligned and homogeneously distributed throughout the ECM construct on the patterned silk substrate (Fig. 4d–f).

hCFs showed much lower potential to generate collagen fibril-based ECM than hCSSCs (Fig. 4g–i), even though seeded on the patterned silk film *with* RGD surface modification. As shown in Fig. 4g, collagen type-I fibrils deposited by hCFs were sparsely distributed on the silk substrate, though maintaining a high level of alignment. The expression of Col-V was also weak (Fig. 4h). Notably, the expression of another key collagen component, Col-VI (Fig. 4i), was comparable to that deposited by hCSSCs (Fig. 4f).

Proteoglycans are other key components of human corneal stromal tissue [48]. Fig. 5(a–i) shows fluorescent confocal imaging of keratan sulfate, lumican, and keratocan (representative proteoglycans in human corneal stroma) deposited by hCSSCs and hCFs on the patterned silk films. Regardless of RGD coupling, the

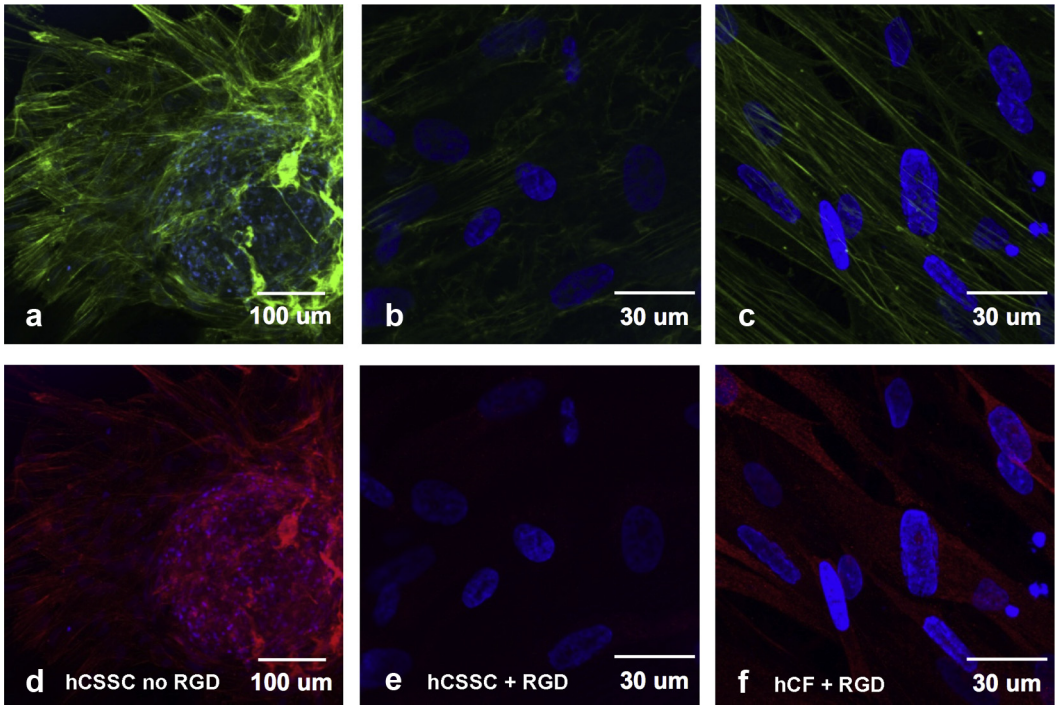

Fig. 3. Comparison of cytoskeletal organization of cultured cells. Micrographs show fluorescent staining of f-actin (green), (a–c) and of α-SMA (red, d–f) in hCSSCs (a,b,d,e) and hCFs (c,f) on the patterned silk films with RGD (b,c,e,f), and without RGD (a,d). Nuclei were stained by DAPI (blue). Images were obtained under identical conditions but spheroid bodies (a,d) are displayed at a lower magnification. (For interpretation of the references to color in this figure legend, the reader is referred to the web version of this article.)

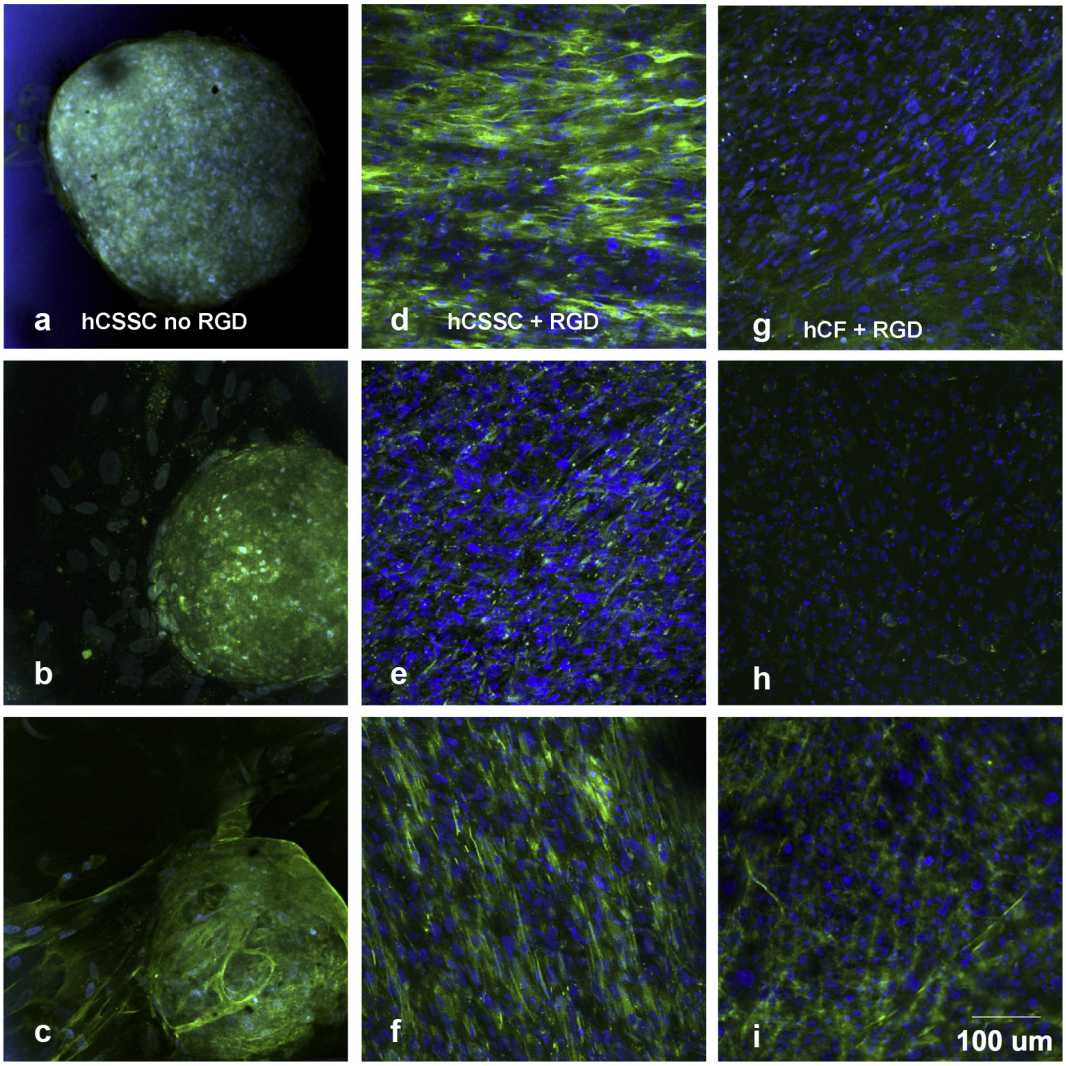

Fig. 4. Collagen deposition in cultured corneal cells. hCSSC cultured on patterned silk substrata without RGD modification (a–c), or with RGD modification (d–f), and hCF on RGD-modified substrata (g–i) after 9 weeks, were immunostained for collagens as described under Methods. Collagen I (a,d,g); collagen V (b,e,h); and collagen VI (c, f, i). Nuclei were stained by DAPI (blue). (For interpretation of the references to color in this figure legend, the reader is referred to the web version of this article.)

expression of these proteoglycans generated by hCSSCs was strong (Fig. 5a–f). With RGD surface coupling, the proteoglycans showed strong alignment (Fig. 5d–f), while without RGD surface coupling, the proteoglycans, like collagen, lacked an orderly structure (Fig. 5a–c). In contrast, the expression of keratan sulfate deposited by hCFs was very weak, and more associated with cell membrane (Fig. 5g). The expression of keratan sulfate proteoglycan protein cores keratocan and lumican were hardly detected (Fig. 5h, i).

3.5. Microstructure of collagenous ECM

Cell morphology and detailed microstructure of elaborated ECM by hCSSCs and hCFs were imaged by electron microscopy and two-photon fluorescence microscopy. The linear grooves alone did not effectively induce hCSSCs to elongate on silk films. As shown in Fig. 6a and d, hCSSCs self-aggregated into isolated cellular spheres (around 100 μm in diameter) surrounded by scattered cells on the linearly grooved silk film *without* RGD surface coupling. No evident collagen fibrils were observed (Fig. 6d). Cultured on silk with RGD surface modification, the hCSSCs were elongated on the linearly grooved silk film and uniformly oriented in the preferred direction (Fig. 6b). There were many dense, fine fibrils between cells on the substrate. The orientation of collagen fibrils was in accordance to hCSSC alignment, and the longitudinal axes of the fibrils were largely parallel to each other. The fibrils were notable in an abundance of small branches. Most of these side branches were free-standing and were not involved in crosslinking the fibrils into an integrated collagen construct (Fig. 6e). Although cultured on the same substrate, hCFs showed an organization distinct from hCSSCs. Elongated hCFs exhibited an orthogonal stratified orientation (shown in the top view, Fig. 6c), consistent with confocal fluorescent imaging observations (Fig. 1g). At higher magnification, hCFs secreted fibrillar ECM that was not well-organized on the patterned substrate (Fig. 6f). Unlike the fibrils secreted by hCSSCs, no side branches were observed. Since without RGD surface coupling the patterned silk substrate did not initialize and guide hCSSCs to deposit organized collagen-fibril construct, we only focused on the samples with RGD surface treatment in the following sections.

As SEM was limited to visualizing only the surface layer of cell-secreted ECM, ECM distribution in *z*-direction was further investigated by two-photon confocal microscopy. Fig. 7 demonstrates the secondary harmonic generation (SHG) signal-visualized collagenous ECM on the patterned silk substrate with surface-coupled RGD. hCSSCs secreted a highly compact collagen-fibrillar

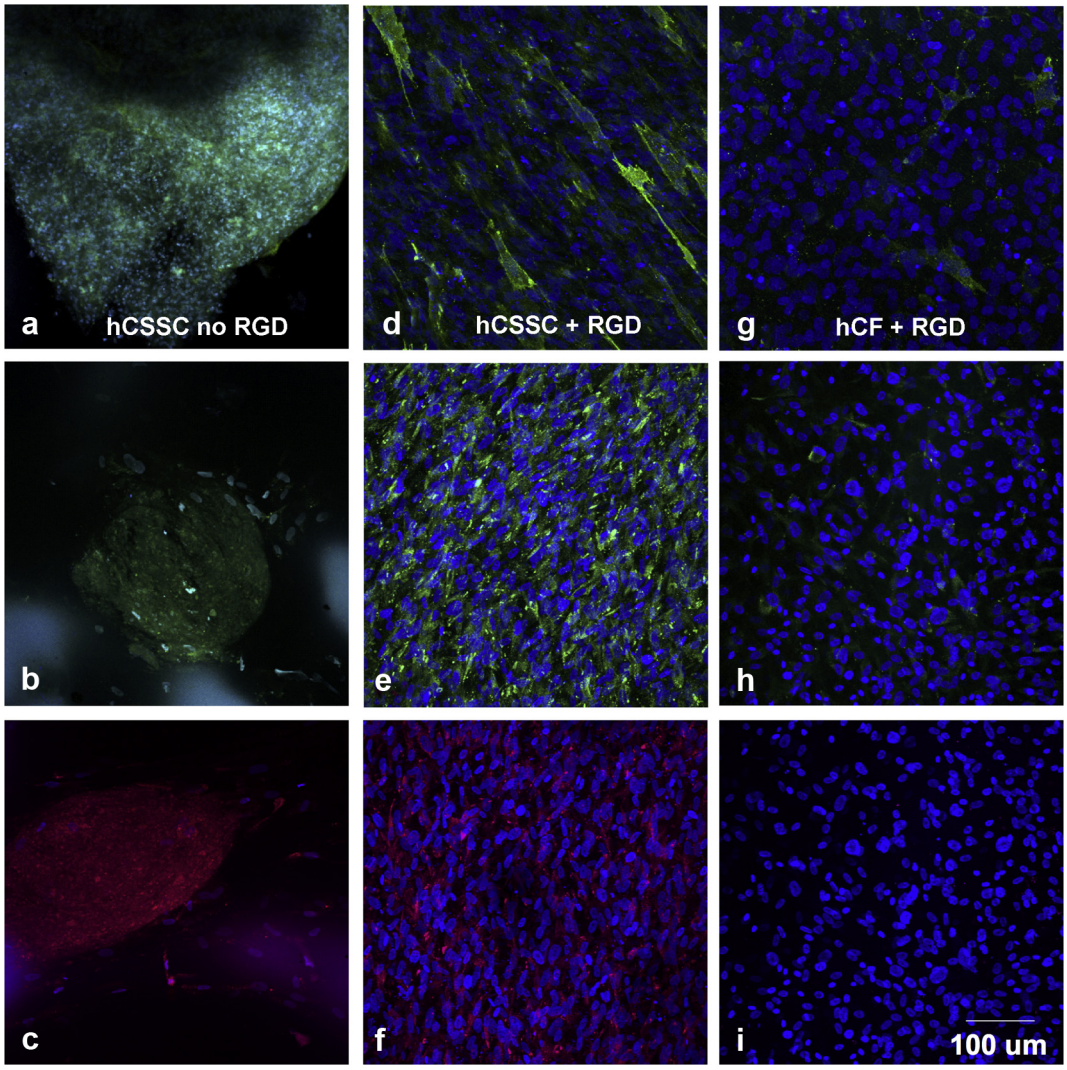

Fig. 5. Immunofluorescence micrographs of corneal stroma-specific proteoglycans. hCSSC without RGD (a–c); hCSSC on RGD (d–f); and hCF on RGD (g–i) were stained after 9 weeks culture on patterned silk films. Proteoglycans (green): Keratan sulfate (a,d,g); Keratocan (b,e,h); Lumican (c, f, i). Nuclei were stained by DAPI (blue). (For interpretation of the references to color in this figure legend, the reader is referred to the web version of this article.)

construct with orthogonal orientations (Fig. 7a). hCFs resembled hCSSCs in generating aligned fibrils with orthogonal orientation, but the construct showed much lower expression of collagen fibrils and sparse layers (Fig. 7b).

TEM micrographs (Fig. 8) revealed the internal microstructure of collagenous ECM secreted by hCSSCs and hCFs on patterned silk substrate *with* RGD surface coupling after 9 week of culture. In hCSSC cultures, most of the cells were located at the top and bottom of the construct, with compressed and flat or oblate morphology. Only a few cells were distributed within the construct (Fig. 8a). hCFs did not form cell layers to sandwich the construct, but tended to integrate into the collagenous ECM and featured ellipsoidal or spindle-like morphology (Fig. 8b). As shown in Fig. 8c the mean thickness of ECM secreted by hCSSCs was 90–100 μm, three fold greater than that of the hCF-secreted ECM. In thin sections, ECM produced by hCSSCs presented stratified, multilayered lamellae with orthogonal fibril orientation (Fig. 8d) where collagen fibrils in one lamella were almost normal to the observation plane (Fig. 8e), and the ones in the adjacent lamella were parallel yet orthogonal (Fig. 8f). The fibril size was uniform, but the inter-fibrillar spacing lacked long-range regularity. For hCFs the collagen fibril bundles crossed each other, but without forming characteristic stratified multi-layer lamellae (Fig. 8g and h). Collagen fibril diameter as a function of cell types is summarized in Fig. 8i. The mean fibril size of ECM secreted by hCSSCs did not significantly differ from that by hCFs (Fig. 8j).

4. Discussion

Due to a lack of cornea donors worldwide, development of a bioengineered human cornea has become a desirable goal as an alternative to penetrating keratoplasty with donated cadaveric tissue. A major obstacle to development of clinically implantable corneal bioequivalents is the bioengineering of stromal tissue. Distinct from the epithelium and endothelium, which are cellular layers supported by basement membranes, the stroma is a highly-organized collagenous connective tissue populated by keratocytes. The stroma is responsible for mechanical strength as well as the refraction and optical transparency of the human cornea. *In vitro* emulation of human corneal stromal tissue is the focus of our tissue engineering strategy.

In previous studies, we demonstrated that a highly aligned PEUU [poly(ε-caprolactone)-based poly (ester urethane) urea] nano-fibrous substrate could serve as a template to initiate and

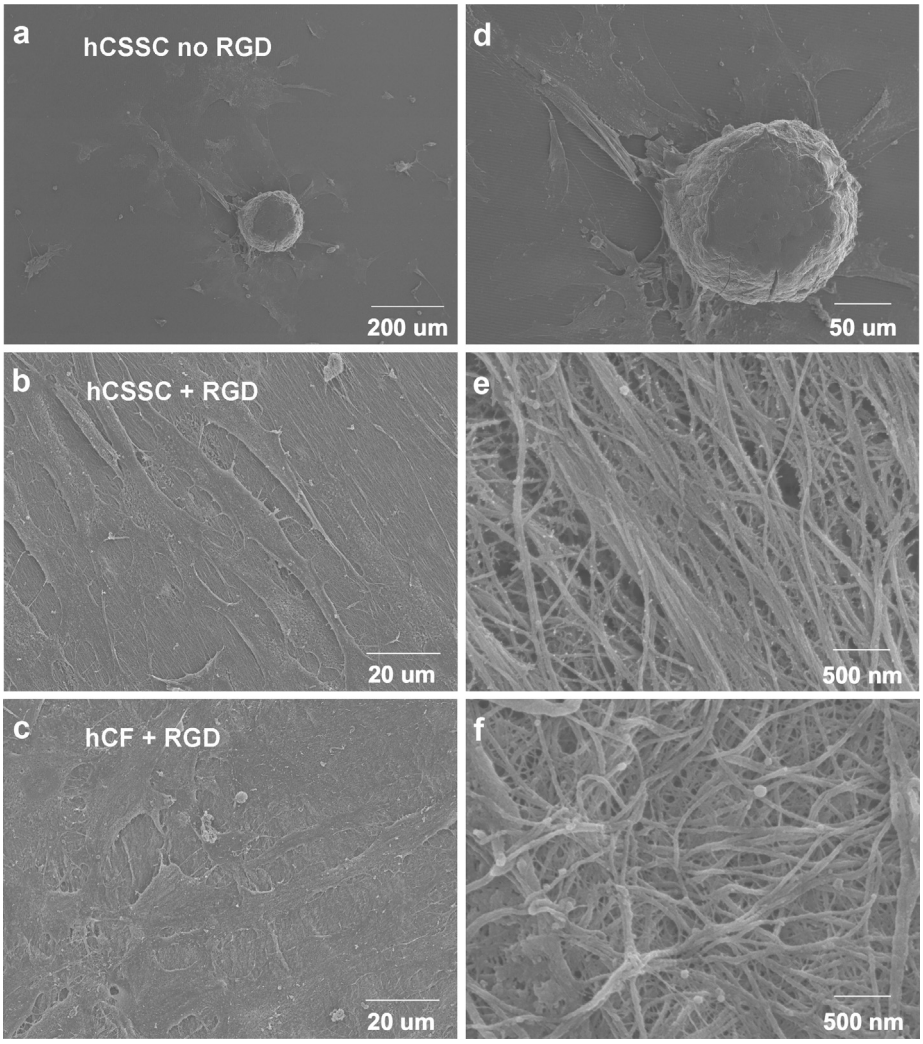

Fig. 6. Scanning electron micrographs of hCSSC cultures (a, b, d, e) and hCF cultures (c, f) on pattered silk films without RGD (a, d) and with RGD (b, c, e, f) surface modification after 9 weeks in culture.

guide the organization of corneal stroma-like tissue by human corneal stromal stem cells [39,40]. The addition of FGF-2 and TGF-β3 successfully stimulated the production of a stromal-like tissue comprised of multilayered lamellae with orthogonally-oriented collagen fibrils and an abundance of cornea-specific proteins and proteoglycans [40]. However, the slow degradation rate and optical opacity limits the use of a PEUU substrate for *in vivo* transplantation. These limitations inspired us to explore a new approach

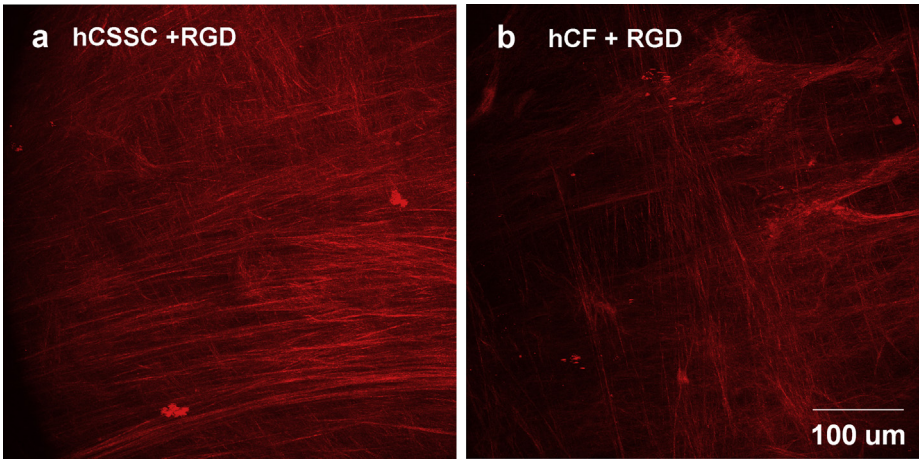

Fig. 7. Two-photon imaging of fibrillar collagen. Fluorescent micrographs of fibrillar collagen were obtained from fixed 9-week cultures of hCSSCs (a) and hCFs (b) on patterned silk films with RGD-surface modification as described in Methods.

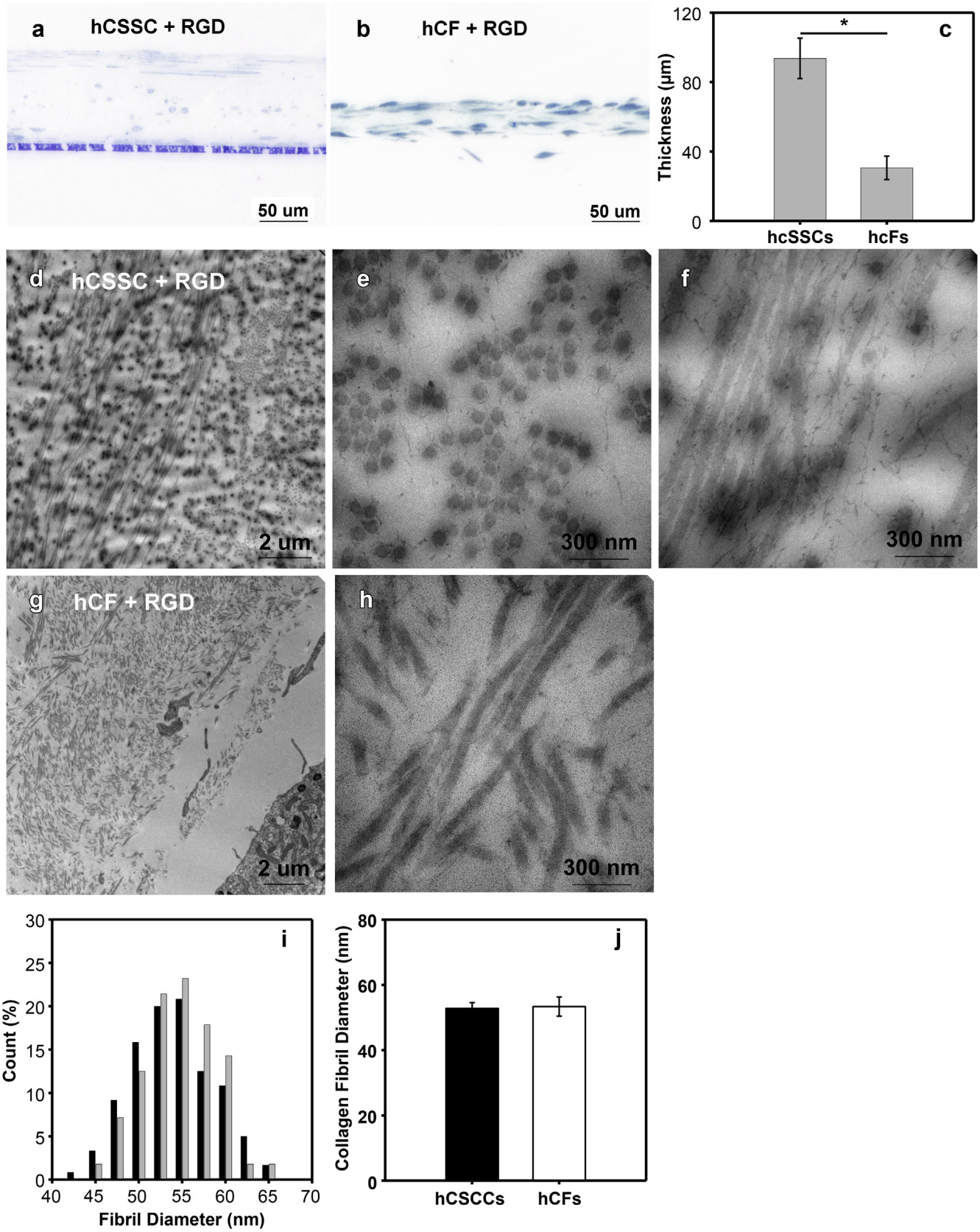

Fig. 8. Distribution and organization of collagen in 9-week cultures. Semi-thin sections of plastic-embedded cultures were stained with toluidine blue to visualize cells (a,b) and thin sections were processed and imaged by transmission electron microscopy as described in Methods to reveal collagen fibrillar arrangement (d–h). Sections from hCSSC cultures are shown in (d–f) and hCF in (g,h). Thickness of the collagen construct was measured from micrographs a and b (c) and collagen fibril diameters measured in multiple sections were compared as described in Methods (i): (black bars) hCSSCs, (gray bars) hCFs. There is no significant difference in collagen fibril diameter between hCSSCs and hCFs (j).

using a more appropriate biomaterial to overcome these shortcomings.

Silk fibroin is a naturally occurring protein extensively used in tissue engineering and regenerative medicine. Its optical transparency, biodegradability and mechanical robustness render silk fibroin films a potentially useful scaffold material for corneal tissue engineering. In a previous study, we demonstrated the importance of topographic cues in initiating and guiding highly ordered collagen fibril nanoconstructs [39]. To facilitate hCSSCs to secrete stroma-like tissue, we patterned silk substrate with linear grooves. Unlike on the aligned PEUU fibrous substrate [40,41], hCSSCs did not align on the unmodified patterned silk substrate. On unmodified fibroin, hCSSCs exhibited a dendritic morphology (Fig. 1a and d) and in differentiation conditions the cells aggregated into spheres (Figs. 4a, b and 6a, d). Spheroid formation has been observed in keratocytes in a culture environment to which the cells have weak attachment to the substratum [52,53].

RGD is a well-known tripeptide ligand for several cellular integrins that mediates cell attachment to ECM proteins containing that amino acid sequence [54–56]. Modification of silk with RGD effectively induced hCSSCs to elongate and align following the linear groove orientation (Fig. 1b). A similar behavior was previously observed for hCFs cultured on similarly patterned silk membrane [25,27], indicating that without effective adhesion between cells and silk substrate, topographic cues alone do not induce cells to elongate and align.

The effect of RGD surface modification was also extended to hCSSCs differentiation to keratocytes and ECM deposition. Fig. 2 demonstrated that, compared with topographic cues alone, RGD induced higher expression of keratocyte-specific gene markers (e.g. ALDH, KERA, CHST6), and lower expressions of myofibroblast-specific gene markers; e.g., EDA-fibronectin (FN-EDA), α-SMA. The mRNA expression levels were reflected in the protein expression and cytoskeletal organization observed by staining of f-actin and α-SMA (Fig. 3). On the patterned silk substrate *with* RGD surface coupling, the ECM produced by hCSSCs was abundant in highly aligned collagen fibrils with high fidelity to hCSSC alignment (Fig. 6b and e).

A similar response to RGD was previously demonstrated by Gil et al. in cultured hCFs [25,27]. RGD surface coupling significantly enhanced transcription expression of some keratocyte markers, including type-I collagen, type-V collagen, decorin and biglycan. Deposition of aligned collagenous ECM was also enhanced. Serum-containing culture medium used in that study tended to maintain a fibroblastic phenotype in the cells. In the current study we explored the possibility that corneal fibroblasts might be reverted to keratocytes, using a serum-free medium we have previously used to induce keratocyte phenotype from stem cells.

However, even in these specialized conditions, hCFs did not differentiate into keratocyte-like cells, but tended to convert into a myofibroblast-like phenotype after 9 weeks of culture. On the patterned silk substrate with RGD surface coupling, hCFs showed an upregulation on FN-EDA and α-SMA expressions when compared to hCSSCs. They also exhibited lower levels of expression of keratocyte marker genes, including KERA and CHST6 (Fig. 2). The pronounced intracellular organization of stress-induced f-actin bundles and α-SMA gave further evidence that hCFs differentiated into a myofibroblast phenotype (Fig. 3c, f).

The differences in cell phenotypes led to the distinct features in the ECM secreted by these cells. hCFs (Fig. 4g, h) showed much weaker type-I and -V collagen protein deposition than hCSSCs (Fig. 4d, e). These are the major fibrillar collagens of cornea and constitute the major structural components of stromal tissue. Similarly, hCFs secreted ECM (Fig. 5g–i) lacking corneal-specific proteoglycan expression, including keratan sulfate, keratocan, and lumican [45,57,58] These molecules have been linked to the regulation of inter-fibril spacing and corneal transparency. ECM produced by hCSSCs, on the other hand (Figs. 4d–f and 5d–f), had abundant components of native human corneal stromal tissue including type-I, -V and -VI collagens, and keratan sulfate, keratocan and lumican.

The differences in the ECM protein expression between these cell types were mirrored in the organization of their respective collagenous ECMs. The lower expression of collagen proteins resulted in much thinner ECM constructs by hCFs (Fig. 8a–c). The former was only one-third of the latter. Surprisingly, there was no significant difference in collagen fibril diameter. Typically, native corneal stroma has one of the smallest diameter fibrillar collagen in the mammalian body and in corneal scars that diameter is much larger. The lack of difference between these two cell types may relate to the ratio of Col-V/Col-I, which is thought to regulate fibril diameter [49–51].

One of the more striking differences in the ECM deposited by the two cell types was the organization of the fibrillar collagen. In normal stroma, the fibrils are tightly packed and arranged in multiple thin layers (lamellae). Such arrangement adds to the strength of the tissue and is thought to be important in maintaining transparency [4,48]. Such a pattern was evident in the collagen produced by hCSSC (Fig. 8d–f), but was clearly absent in the collagen deposited by the hCF cells (Fig. 8g, h).

Collagen organization in the stroma has been attributed to the presence of a unique family of proteoglycans containing the proteins lumican and keratocan modified with high molecular weight keratan sulfate. The absence of keratan sulfate results in disruption of stromal microstructure in the disease Macular Corneal Dystrophy [59,60]. Knockout of lumican also leaves mouse corneas cloudy due to collagen fibril disorganization [58,61,62]. Even though hCFs align and express some typical keratocyte marker genes, under cell culture conditions they do not regain the proteoglycan synthesis characteristic of keratocytes. Thus we speculate that, like the cornea *in vivo*, assembling appropriate stromal architecture depends on collagen synthesis, which is not tissue specific, but also on expression of some or all of the unique array of corneal proteoglycans produced by hCSSCs but absent in hCF cultures.

Stroma of the adult human cornea is more than 500 μm in thickness. The constructs produced by hCSSC on silk membranes and on polymeric nanofiber substrata are only about 1/6 of this dimension. However, because the silk substrata are transparent and biocompatible, the current study opens the door to assembling full thickness bioengineered stromal tissue by stacking individual constructs obviating the need to remove the substratum from the tissue construct. The fibroin protein would presumably degrade over time leaving a native lamellar stromal tissue fully populated with human keratocytes. Learning to assemble such tissue constructs would appear to be the next step in use of silk protein substrata to engineer corneal tissue using stem cells.

5. Conclusions

We compared human corneal stromal stem cells (hCSSCs) with human corneal fibroblasts (hCFs) in generation of human corneal stromal tissue employing a combination of surface guidance and growth factor supplementation. After culture in KDM, hCSSCs successfully differentiated into keratocyte-like cells with substantial up-regulated expression of keratocyte gene markers (*KERA, PTDGS, ALDH, CHST6*), and deposited ECM abundant in collagen type-I as well as Col-V, Col-VI, keratan sulfate, lumican and keratocan, typifying the ECM of the corneal stroma on the patterned silk substrates with RGD surface modification. On the contrary, hCFs tended to differentiate into myofibroblast-like cells, and secreted

an ECM lacking cornea-specific components. The construct from hCSSCs was 90–100 μm in thickness and featured stratified multilayered collagen-fibril lamellae with orthogonal orientation, morphologically close to that of native human corneal stromal tissue. ECM secreted by hCFs was only 20–30 μm thick and lacked the orderly organization in the pattern of corneal scar-like tissue. These observations support the idea that patterned silk substrate with RGD surface coupling could serve as an amenable microenvironment to induce hCSSCs to develop an artificial bioequivalent of human corneal stromal tissue.

Acknowledgments

The authors would like to thank Dr. Simon C. Watkins, Mr. Gregory Gibson and Mrs. Ming Sun form Center of Biologic Imaging (CBI) of University of Pittsburgh for their support and assistance in two-photon microscopy and sample preparation for transmission electron microscopy (TEM). This work was supported by the Ocular Tissue Engineering and Regenerative Ophthalmology (OTERO) program of the UPMC Eye Center and the McGowan Institute for Regenerative Medicine, Research to Prevent Blindness Inc, NIH grant P30-EY08098, EY016415 (to JLF) and EY020856 (DLK).

References

[1] Eye Bank Association of America. 2012 eye banking statistical report. EBAA; 2013. http://www.restoresight.org.
[2] Borderie VM, Boelle PY, Touzeau O, Allouch C, Boutboul S, Laroche L. Predicted long-term outcome of corneal transplantation. Ophthalmology 2009;116:2354–60.
[3] Shah A, Brugnano J, Sun S, Vase A, Orwin E. The development of a tissue-engineered cornea: biomaterials and culture methods. Pediatr Res 2008;63:535–44.
[4] Ruberti JW, Zieske JD. Prelude to corneal tissue engineering - gaining control of collagen organization. Prog Retin Eye Res 2008;27:549–77.
[5] Germain L, Carrier P, Auger FA, Salesse C, Guerin SL. Can we produce a human corneal equivalent by tissue engineering? Prog Retin Eye Res 2000;19:497–527.
[6] Tan DT, Dart JK, Holland EJ, Kinoshita S. Corneal transplantation. Lancet 2012;379:1749–61.
[7] Maurice DM. The structure and transparency of the cornea. J Physiol 1957;136:263–86.
[8] Ruberti JW, Roy AS, Roberts CJ. Corneal biomechanics and biomaterials. Annu Rev Biomed Eng 2011;13:269–95.
[9] Benedek GB. Theory of transparency of the eye. Appl Opt 1971;10:459–73.
[10] Panilaitis B, Altman GH, Chen J, Jin HJ, Karageorgiou V, Kaplan DL. Macrophage responses to silk. Biomaterials 2003;24:3079–85.
[11] Meinel L, Hofmann S, Karageorgiou V, Kirker-Head C, McCool J, Gronowicz G, et al. The inflammatory responses to silk films in vitro and in vivo. Biomaterials 2005;26:147–55.
[12] Wang Y, Rudym DD, Walsh A, Abrahamsen L, Kim HJ, Kim HS, et al. In vivo degradation of three-dimensional silk fibroin scaffolds. Biomaterials 2008;29:3415–28.
[13] Jin HJ, Park J, Karageorgiou V, Kim UJ, Valluzzi R, Cebe P, et al. Water-stable silk films with reduced β-sheet content. Adv Funct Mater 2005;15:1241–7.
[14] Motta A, Fambri L, Migliaresi C. Regenerated silk fibroin films: Thermal and dynamic mechanical analysis. Macromol Chem Phys 2002;203:1658–65.
[15] Shao Z, Vollrath F. Surprising strength of silkworm silk. Nature 2002;418:741.
[16] Kim HJ, Kim UJ, Vunjak-Novakovic G, Min BH, Kaplan DL. Influence of macroporous protein scaffolds on bone tissue engineering from bone marrow stem cells. Biomaterials 2005;26:4442–52.
[17] Harkin DG, George KA, Madden PW, Schwab IR, Hutmacher DW, Chirila TV. Silk fibroin in ocular tissue reconstruction. Biomaterials 2011;32:2445–58.
[18] Harkin DG, Chirila TV. Silk fibroin in ocular surface reconstruction: what is its potential as a biomaterial in ophthalmics? Future Med Chem 2012;4:2145–7.
[19] Liu J, Lawrence BD, Liu A, Schwab IR, Oliveira LA, Rosenblatt MI. Silk fibroin as a biomaterial substrate for corneal epithelial cell sheet generation. Invest Ophthalmol Vis Sci 2012;53:4130–8.
[20] Chirila T, Barnard Z, Zainuddin, Harkin DG, Schwab IR, Hirst L. *Bombyx mori* silk fibroin membranes as potential substrata for epithelial constructs used in the management of ocular surface disorders. Tissue Eng Part A 2008;14:1203–11.
[21] Bray LJ, George KA, Ainscough SL, Hutmacher DW, Chirila TV, Harkin DG. Human corneal epithelial equivalents constructed on *Bombyx mori* silk fibroin membranes. Biomaterials 2011;32:5086–91.
[22] Madden PW, Lai JN, George KA, Giovenco T, Harkin DG, Chirila TV. Human corneal endothelial cell growth on a silk fibroin membrane. Biomaterials 2011;32:4076–84.
[23] Shadforth AM, George KA, Kwan AS, Chirila TV, Harkin DG. The cultivation of human retinal pigment epithelial cells on *Bombyx mori* silk fibroin. Biomaterials 2012;33:4110–7.
[24] Higa K, Takeshima N, Moro F, Kawakita T, Kawashima M, Demura M, et al. Porous silk fibroin film as a transparent carrier for cultivated corneal epithelial sheets. J Biomater Sci Polym Ed 2011;22:2261–76.
[25] Lawrence BD, Marchant JK, Pindrus MA, Omenetto FG, Kaplan DL. Silk film biomaterials for cornea tissue engineering. Biomaterials 2009;30:1299–308.
[26] Gil ES, Park SH, Marchant J, Omenetto F, Kaplan DL. Response of human corneal fibroblasts on silk film surface patterns. Macromol Biosci 2010;10:664–73.
[27] Gil ES, Mandal BB, Park SH, Marchant JK, Omenetto FG, Kaplan DL. Helicoidal multi-lamellar features of RGD-functionalized silk biomaterials for corneal tissue engineering. Biomaterials 2010;31:8953–63.
[28] Chen J, Altman GH, Karageorgiou V, Horan R, Collette A, Volloch V, et al. Human bone marrow stromal cell and ligament fibroblast responses on RGD-modified silk fibers. J Biomed Mater Res A 2003;67:559–70.
[29] Long CJ, Roth MR, Tasheva ES, Funderburgh M, Smit R, Conrad GW, et al. Fibroblast growth factor-2 promotes keratan sulfate proteoglycan expression by keratocytes in vitro. J Biol Chem 2000;275:13918–23.
[30] Jester JV, Barry-Lane PA, Cavanagh HD, Petroll WM. Induction of alpha-smooth muscle actin expression and myofibroblast transformation in cultured corneal keratocytes. Cornea 1996;15:505–16.
[31] Espana EM, He H, Kawakita T, Di Pascuale MA, Raju VK, Liu CY, et al. Human keratocytes cultured on amniotic membrane stroma preserve morphology and express keratocan. Invest Ophthalmol Vis Sci 2003;44:5136–41.
[32] Beales MP, Funderburgh JL, Jester JV, Hassell JR. Proteoglycan synthesis by bovine keratocytes and corneal fibroblasts: maintenance of the keratocyte phenotype in culture. Invest Ophthalmol Vis Sci 1999;40:1658–63.
[33] Funderburgh JL, Funderburgh ML, Mann MM, Corpuz L, Roth MR. Proteoglycan expression during transforming growth factor beta -induced keratocyte-myofibroblast transdifferentiation. J Biol Chem 2001;276:44173–8.
[34] Pinnamaneni N, Funderburgh JL. Concise review: stem cells in the corneal stroma. Stem Cells 2012;30:1059–63.
[35] Du Y, Sundarraj N, Funderburgh ML, Harvey SA, Birk DE, Funderburgh JL. Secretion and organization of a cornea-like tissue in vitro by stem cells from human corneal stroma. Invest Ophthalmol Vis Sci 2007;48:5038–45.
[36] Du Y, Funderburgh ML, Mann MM, SundarRaj N, Funderburgh JL. Multipotent stem cells in human corneal stroma. Stem Cells 2005;23:1266–75.
[37] Du Y, Carlson EC, Funderburgh ML, Birk DE, Pearlman E, Guo N, et al. Stem cell therapy restores transparency to defective murine corneas. Stem Cells 2009;27:1635–42.
[38] Rockwood DN, Preda RC, Yucel T, Wang X, Lovett ML, Kaplan DL. Materials fabrication from *Bombyx mori* silk fibroin. Nat Protoc 2011;6:1612–31.
[39] Wu J, Du Y, Watkins SC, Funderburgh JL, Wagner WR. The engineering of organized human corneal tissue through the spatial guidance of corneal stromal stem cells. Biomaterials 2012;33:1343–52.
[40] Wu J, Du Y, Mann MM, Yang E, Funderburgh JL, Wagner WR. Bioengineering organized, multilamellar human corneal stromal tissue by growth factor supplementation on highly aligned synthetic substrates. Tissue Eng Part A 2013;19:2063–75.
[41] Funderburgh JL, Mann MM, Funderburgh ML. Keratocyte phenotype mediates proteoglycan structure: a role for fibroblasts in corneal fibrosis. J Biol Chem 2003;278:45629–37.
[42] Berryhill BL, Beales MP, Hassell JR. Production of prostaglandin D synthase as a keratan sulfate proteoglycan by cultured bovine keratocytes. Invest Ophthalmol Vis Sci 2001;42:1201–7.
[43] Di Iorio E, Barbaro V, Volpi N, Bertolin M, Ferrari B, Fasolo A, et al. Localization and expression of CHST6 and keratan sulfate proteoglycans in the human cornea. Exp Eye Res 2010;91:293–9.
[44] Pei Y, Reins RY, McDermott AM. Aldehyde dehydrogenase (ALDH) 3A1 expression by the human keratocyte and its repair phenotypes. Exp Eye Res 2006;83:1063–73.
[45] Qin D, Xia Y, Whitesides GM. Soft lithography for micro- and nanoscale patterning. Nat Protoc 2010;5:491–502.
[46] Tien LW, Gil ES, Park SH, Mandal BB, Kaplan DL. Patterned silk film scaffolds for aligned lamellar bone tissue engineering. Macromol Biosci 2012;12:1671–9.
[47] Zimmermann DR, Trueb B, Winterhalter KH, Witmer R, Fischer RW. Type VI collagen is a major component of the human cornea. FEBS Lett 1986;197:55–8.
[48] Hassell JR, Birk DE. The molecular basis of corneal transparency. Exp Eye Res 2010;91:326–35.
[49] Birk DE, Fitch JM, Linsenmayer TF. Organization of collagen types I and V in the embryonic chicken cornea. Invest Ophthalmol Vis Sci 1986;27:1470–7.
[50] Birk DE, Fitch JM, Babiarz JP, Doane KJ, Linsenmayer TF. Collagen fibrillogenesis in vitro: interaction of types I and V collagen regulates fibril diameter. J Cell Sci 1990;95(Pt 4):649–57.
[51] Birk DE. Type V collagen: heterotypic type I/V collagen interactions in the regulation of fibril assembly. Micron 2001;32:223–37.
[52] Lai JY, Tu IH. Adhesion, phenotypic expression, and biosynthetic capacity of corneal keratocytes on surfaces coated with hyaluronic acid of different molecular weights. Acta Biomater 2012;8:1068–79.
[53] Funderburgh ML, Mann MM, Funderburgh JL. Keratocyte phenotype is enhanced in the absence of attachment to the substratum. Mol Vis 2008;14:308–17.

[54] Ruoslahti E. RGD and other recognition sequences for integrins. Annu Rev Cell Dev Biol 1996;12:697–715.
[55] D'Souza SE, Ginsberg MH, Plow EF. Arginyl-glycyl-aspartic acid (RGD): a cell adhesion motif. Trends Biochem Sci 1991;16:246–50.
[56] Ruoslahti E, Pierschbacher MD. New perspectives in cell adhesion: RGD and integrins. Science 1987;238:491–7.
[57] Funderburgh JL. Keratan sulfate: structure, biosynthesis, and function. Glycobiology 2000;10:951–8.
[58] Kao WW, Liu CY. Roles of lumican and keratocan on corneal transparency. Glycoconj J 2002;19:275–85.
[59] Klintworth GK, Meyer R, Dennis R, Hewitt AT, Stock EL, Lenz ME, et al. Macular corneal dystrophy. Lack of keratan sulfate in serum and cornea. Ophthalmic Paediatr Genet 1986;7:139–43.
[60] Klintworth GK. Corneal dystrophies. Orphanet J Rare Dis 2009;4:7.
[61] Kao WW, Funderburgh JL, Xia Y, Liu CY, Conrad GW. Focus on molecules: lumican. Exp Eye Res 2006;82:3–4.
[62] Chakravarti S, Petroll WM, Hassell JR, Jester JV, Lass JH, Paul J, et al. Corneal opacity in lumican-null mice: defects in collagen fibril structure and packing in the posterior stroma. Invest Ophthalmol Vis Sci 2000;41:3365–73.